Bright Soliton to Quantum Droplet Transition in a Mixture of Bose-Einstein Condensates

P. Cheiney, C. R. Cabrera, J. Sanz, B. Naylor, L. Tanzi, and L. Tarruell*
ICFO—Institut de Ciencies Fotoniques, The Barcelona Institute of Science and Technology, 08860 Castelldefels (Barcelona), Spain

(Received 30 October 2017; published 27 March 2018)

Attractive Bose-Einstein condensates can host two types of macroscopic self-bound states: bright solitons and quantum droplets. Here, we investigate the connection between them with a Bose-Bose mixture confined in an optical waveguide. We show theoretically that, depending on atom number and interaction strength, solitons and droplets can be smoothly connected or remain distinct states coexisting only in a bistable region. We measure their spin composition, extract their density for a broad range of parameters, and map out the boundary of the region separating solitons from droplets.

DOI: 10.1103/PhysRevLett.120.135301

Self-bound states are ubiquitous in nature, and appear in contexts as diverse as solitary waves in channels, optical solitons in nonlinear media, and liquid He droplets [1–3]. Their binding results from a balance between attractive forces, which tend to make the system collapse, and repulsive ones, which stabilize it to a finite size.

Bose-Einstein condensates (BECs) with attractive mean-field interactions constitute ideal model systems to explore in the same setting self-bound states stabilized by repulsive forces of different classes. On the one hand, bright solitons in optical waveguides have been observed with ^{7}Li [4–6], ^{85}Rb [7–9], and ^{39}K atoms [10]. These matter-wave analogues of optical solitons are stabilized against collapse by the dispersion along the unconfined direction, which is a (single-particle) kinetic effect. On the other hand, quantum droplets—self-bound clusters of atoms with liquid-like properties—have been recently demonstrated with ^{164}Dy [11–14] and ^{166}Er atoms [15], and in mixtures of ^{39}K BECs [16]. In this case, the repulsive force preventing the collapse stems from quantum fluctuations, and has a quantum many-body origin [17].

Bright solitons and quantum droplets are *a priori* distinct states which exist in very different regimes. Solitons require the gas to remain effectively one dimensional, which limits their maximal atom number [18–20]. In contrast, droplets are three-dimensional solutions that exist even in free space and require a minimum atom number to be stable [14–17,21,22]. Up to now, quantum droplet experiments focused exclusively on systems where solitons were absent, enabling an unambiguous identification of the droplet state. Therefore, they could not provide any insights on their connections to solitons.

In this Letter, we bridge this gap by exploring a system that can host both bright solitons and quantum droplets: a mixture of two BECs in an optical waveguide. We observe that, as soon as the mean-field interactions become effectively attractive, self-bound states of well-defined spin composition appear. We show theoretically that their nature evolves from solitonlike to dropletlike upon increase of the atom number. Depending on the interaction strength, both regimes can be smoothly connected, or remain distinct states that coexist only in a bistable region. We determine experimentally their density for a broad range of atom numbers and interaction strengths, and map out the boundary of the bistable region that separates bright solitons from quantum droplets.

We perform experiments with a mixture of ^{39}K BECs in Zeeman states $|\uparrow\rangle \equiv |m_F = -1\rangle$ and $|\downarrow\rangle \equiv |m_F = 0\rangle$ of the $F = 1$ hyperfine manifold. The optical waveguide is created by a red-detuned optical dipole trap of radial trapping frequency $\omega/2\pi = 109(1)$ Hz, see inset of Fig. 1(a). The system is imaged *in situ* with a spatial resolution of the order of the harmonic oscillator length $a_{\mathrm{ho}} = \sqrt{\hbar/m\omega} \simeq 1.5$ μm,

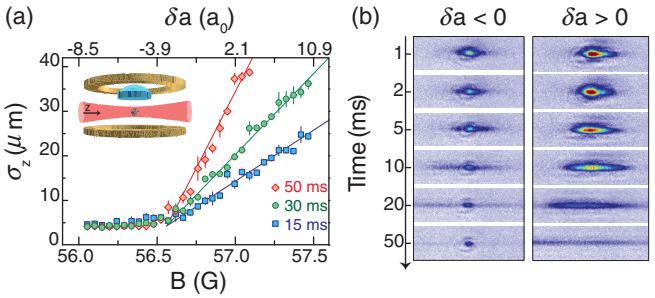

FIG. 1. Self-bound states. (a) Gaussian $1/e$ width σ_z of the mixture as a function of the magnetic field B (corresponding to different values of δa), for various evolution times after release in the optical waveguide (inset). For $B < 56.6$ G the system becomes self-bound and σ_z saturates to the imaging resolution. Solid lines are linear fits to the data in the expanding regime and error bars denote the standard deviation of 10 independent measurements. (b) Typical *in situ* images for increasing evolution times, corresponding to a self-bound state (expanding gas) in the attractive (repulsive) regime with $\delta a < 0$ ($\delta a > 0$) and initial atom number $N \sim 7000$ ($N \sim 30000$).

with $\hbar$ the reduced Planck constant and m the mass of ^{39}K. We exploit a phase-contrast polarization scheme [23] to image both states with the same sensitivity [16]. The interactions are tuned *via* magnetic Feshbach resonances and parametrized by the intra- and intercomponent scattering lengths $a_{\uparrow\uparrow}, a_{\downarrow\downarrow} > 0$ and $a_{\uparrow\downarrow} < 0$ [24]. Assuming that both components occupy the same spatial mode with a density ratio $n_\uparrow/n_\downarrow = \sqrt{a_{\downarrow\downarrow}/a_{\uparrow\uparrow}}$, the overall mean-field interaction is proportional to $\delta a = a_{\uparrow\downarrow} + \sqrt{a_{\uparrow\uparrow}a_{\downarrow\downarrow}}$, which is attractive for $B < 56.84$ G [25].

The experiment starts with a pure BEC in state $|\uparrow\rangle$ confined in a crossed optical dipole trap of frequencies $\omega_{x,y,z}/2\pi = [119(1), 109(1), 49(1)]$ Hz. A radio-frequency (rf) pulse is used to prepare a controlled mixture of the two components [37]. The pulse is performed at $B \sim 57.2$ G, where $\delta a > 0$ and the system is in the miscible regime [38]. Subsequently the magnetic field is ramped down at a constant rate of 11.8 G/s while reducing the longitudinal confinement. The latter is removed in 5 ms at the final magnetic field, leaving the system unconfined along the z direction [39].

Figure 1(b) shows typical *in situ* images of the time evolution of the mixture after release in the optical waveguide. Figure 1(a) displays its longitudinal size σ_z as a function of magnetic field, for three different evolution times. In the repulsive regime ($\delta a > 0$) σ_z increases with δa, reflecting the increase of the released energy of the gas. In contrast, in the attractive regime ($\delta a < 0$) the absence of expansion indicates the existence of self-bound states. Experimentally, we only observe this behavior below $\delta a \sim -2a_0$, where a_0 denotes the Bohr radius. As in Ref. [10], we attribute this effect to the initial confinement energy of the system.

The observed self-bound states are intrinsically composite objects, involving both $|\uparrow\rangle$ and $|\downarrow\rangle$ atoms. To probe this aspect, we prepare mixtures of different compositions by varying the rf pulse time τ. Large population imbalances between the two states result in bimodal density profiles in the *in situ* images, see left panel of Fig. 2(a). They consist of a self-bound state surrounded by a wider and expanding cloud of atoms of the excess component. We find that the fraction of self-bound atoms is maximized for an optimal pulse time, see central panel.

To determine its spin composition we perform a complementary set of measurements, modifying the detection sequence. We dissociate the self-bound state by increasing the magnetic field to the repulsive regime ($B \sim 57.3$ G) in 1 ms, similar to Ref. [11]. We then measure the atom number per spin component $N_\uparrow$ and $N_\downarrow$ via Stern-Gerlach separation during time-of-flight expansion, see right panel. We extract the optimal composition as a function of B by combining the *in situ* and time-of-flight measurements, see Fig. 2(b). The interaction energy of the system is minimized by maximizing the spatial overlap of the two components [17,40]. The theoretical prediction, assuming that both occupy the same spatial mode, yields $N_\uparrow/N_\downarrow = \sqrt{a_{\downarrow\downarrow}/a_{\uparrow\uparrow}}$ (solid line), which is in fair agreement with the data.

To clarify the nature of the self-bound states and their relation to the well-known bright soliton and quantum droplet limits, we perform a theoretical analysis of the system. It is based on the extended Gross-Pitaevskii equation (EGPE) proposed in Ref. [17], which includes the effect of quantum fluctuations through an additional repulsive term. We examine the case where $N_\uparrow/N_\downarrow = \sqrt{a_{\downarrow\downarrow}/a_{\uparrow\uparrow}}$ and assume explicitly that the two components occupy the same spatial mode $\Psi_\uparrow = \sqrt{n_\uparrow}\phi$ and $\Psi_\downarrow = \sqrt{n_\downarrow}\phi$, where $n_0 = n_\uparrow + n_\downarrow$ is the total peak density of the system and $n_\uparrow/n_\downarrow = \sqrt{a_{\downarrow\downarrow}/a_{\uparrow\uparrow}}$ [41]. The system is then described by

$$i\hbar\dot{\phi} = \left[\left(-\frac{\hbar^2}{2m}\nabla^2 + V_{\mathrm{trap}}\right) + \alpha n_0|\phi|^2 + \gamma n_0^{3/2}|\phi|^3\right]\phi, \quad (1)$$

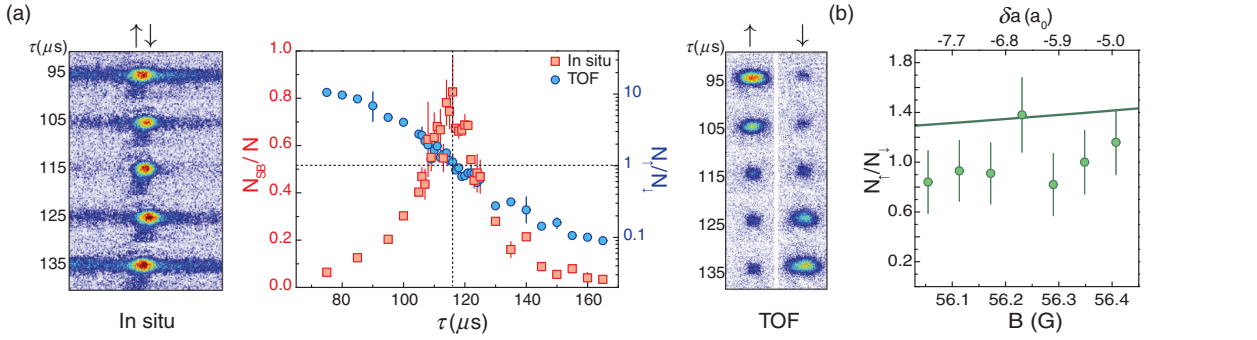

FIG. 2. Spin composition. (a) Left panel: *In situ* images of the mixture for various rf pulse times τ and $B = 56.35(1)$ G. Away from an optimal value the density profile is bimodal, with a self-bound state surrounded by atoms of the excess component. Central panel: Fraction of self-bound atoms N_{SB}/N (red squares) and spin composition $N_\uparrow/N_\downarrow$ (blue circles) as a function of τ. Error bars denote the standard deviation of 4 measurements. Right panel: Corresponding time-of-flight (TOF) Stern-Gerlach analysis of the spin composition. (b) Optimal ratio $N_\uparrow/N_\downarrow$ as a function of magnetic field B. Error bars correspond to the confidence interval of the fit [25]. The solid line depicts the theoretical prediction $N_\uparrow/N_\downarrow = \sqrt{a_{\downarrow\downarrow}/a_{\uparrow\uparrow}}$.

where V_{trap} denotes the waveguide confinement, and $\alpha \propto \delta a$ and $\gamma \propto (\sqrt{a_{\uparrow\uparrow} a_{\downarrow\downarrow}})^{5/2}$ are functions of the magnetic field [25]. Note that although this equation bears strong similarities with the cubic-quintic nonlinear Schrödinger equation employed in optics to describe high-order material nonlinearities [2], the repulsive term has an unusual quartic dependence. This is the scaling corresponding to quantum fluctuations in three-dimensional condensates [42], which is the regime explored experimentally [43].

We compute the ground state of the system by solving numerically the EGPE [25]. The left panel of Fig. 3(a) depicts its peak density n_0 as a function of the total atom number $N = N_\uparrow + N_\downarrow$ and magnetic field B (equivalently, interaction strength δa). For large attraction we find two distinct behaviors: a high-density solution ($n_0 \sim 10^{16}$ atoms/cm^3) for large N, and a low-density one ($n_0 \sim 10^{13}$ atoms/cm^3) for small N. In between, the gray region corresponds to a bistable regime where both solutions are possible. Its boundaries are signaled by a discontinuity of the density. This behavior disappears above a critical magnetic field ($B_c \sim 55.85$ G for our experimental confinement). Beyond, the system supports a single solution whose density increases progressively with N. This situation is analogous to a quantum ($T = 0$) first order liquid-to-gas phase transition: the bistable regime contains metastable regions surrounding a transition line, and a crossover region appears above B_c.

For all parameters considered in Fig. 3(a), we find that the density profile of the system is well approximated by a Gaussian. To gain further insight on the phase diagram, we thus perform a variational analysis of the EGPE [44] introducing the ansatz $\phi = e^{-r^2/2\sigma_r^2 - z^2/2\sigma_z^2}$ [25]. Figure 3(b) displays the energy landscapes obtained at a fixed magnetic field $B = 55.6$ G $< B_c$. For small values of N (bottom row), the energy has a single minimum corresponding to a dilute and elongated cloud: a composite bright soliton. Its radial size σ_r corresponds to the harmonic oscillator length a_{ho}, and its longitudinal size σ_z and energy E are similar to those obtained in a mean-field treatment without quantum fluctuations (bottom right panel, gray dotted line). For large values of N (top row) the minimum corresponds to a dense and isotropic solution with $\sigma_r \ll a_{\mathrm{ho}}$: a quantum liquid droplet. Its properties are not affected by the trapping potential, and it exists in its absence (top right panel, gray dashed line). In the bistable region (central row) both composite bright solitons and liquid droplets exist simultaneously. Above the critical magnetic field B_c a crossover takes place, with a single solution which evolves from solitonlike to dropletlike upon increasing the atom number [45].

We explore experimentally the phase diagram of the system preparing self-bound states at different interaction strengths, starting from the high N regime. We observe that their atom number decreases in time due to inelastic processes, see Fig. 3(c). For our experimental parameters

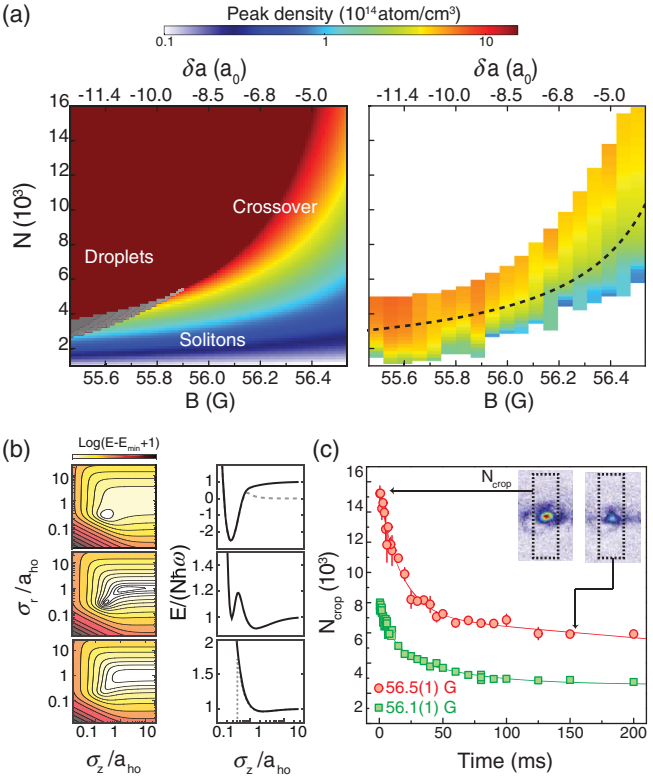

FIG. 3. Soliton-to-droplet diagram. (a) Left panel: Ground state peak density vs atom number N and magnetic field B computed numerically from the EGPE. Solitons and droplets are distinct solutions, which coexist in a bistable region (gray area) and become smoothly connected in the crossover above $B_c \sim 55.85$ G. Right panel: Peak density extracted from the decay of the self-bound atom number, see (c). Self-bound states are stabilized by beyond mean-field effects well above the mean-field collapse threshold for composite bright solitons (dashed line). (b) Left panel: Energy E of the system predicted by a Gaussian variational ansatz as a function of the radial σ_r and longitudinal σ_z sizes, for $B = 55.6$ G and $N = 6000$ (top, droplet), $N = 3700$ (center, bistable region) and $N = 2500$ (bottom, soliton). Right panel: Corresponding one-dimensional cuts along σ_z, for the value of σ_r that minimizes E. All panels, solid lines: solution of the complete model; top panel, gray dashed line: solution in the absence of optical waveguide; bottom panel, gray dotted line: solution in the absence of quantum fluctuations. (c) Evolution of the self-bound atom number N_{crop}, determined from the zeroth moment of the cropped region (insets), as a function of time t. Solid lines: empirical fit for extracting the decay rate [25]. Error bars: Standard deviation of 4 measurements.

these are completely dominated by three-body recombination in the $\downarrow\downarrow\downarrow$ channel [25]. We model the decay of the self-bound atom number using the simplified rate equation $\dot{N}/N = -K_3^{\mathrm{eff}} \langle n^2 \rangle$, where $\langle n^2 \rangle$ is the total mean square density and K_3^{eff} an effective three-body loss coefficient. The model assumes that the $|\downarrow\rangle$ losses are accompanied by the expulsion of $|\uparrow\rangle$ atoms from the self-bound state in order to maintain the value of $N_\uparrow/N_\downarrow$ constant [25].

Similarly to recent experiments on dipolar ^{166}Er droplets [15], we extract the density of the self-bound state by measuring the decay of its atom number. The latter allows us to map out the density as a function of N from a single decay curve, overcoming the limits set by the imaging resolution [46]. The right panel of Fig. 3(a) displays the determined peak densities as a function of atom number and magnetic field. Interestingly, a large fraction of the measurements lies well above the mean-field bright soliton collapse threshold. At the theoretical optimum for $N_\uparrow/N_\downarrow$ it corresponds to the condition $N_c = 0.6268 a_{\mathrm{ho}}(1+\sqrt{a_{\downarrow\downarrow}/a_{\uparrow\uparrow}})^2/(2|\delta a|\sqrt{a_{\downarrow\downarrow}/a_{\uparrow\uparrow}})$ (dashed line) [25]. The absence of collapse in our measurements shows the existence of a stabilizing beyond mean-field mechanism.

In the deeply bound regime the measured peak densities agree only qualitatively with the EGPE predictions, see left and right panels of Fig. 3(a). The discrepancies might stem from two sources. First, we have considered that the spin composition of the system adjusts to $N_\uparrow/N_\downarrow = \sqrt{a_{\downarrow\downarrow}/a_{\uparrow\uparrow}}$ while we have seen experimentally that population imbalances are possible. Second, our decay model is very simplified and assumes that the $|\downarrow\rangle$ losses are immediately accompanied by the disappearance of $|\uparrow\rangle$ atoms when, in reality, these require a finite time to exit the observation region.

In a last series of experiments we explore the phase diagram by approaching the bistability region from the soliton regime, see left inset of Fig. 4(a). We prepare the system in the crossover region at $B \sim 56.3$ G and hold it in the crossed optical dipole trap for a variable time (1–120 ms). Owing to three-body recombination, this results in atom numbers $N = 3000$ to 7000. We then remove the vertical trapping beam, rapidly decrease B to its final value at a rate of 93.8 G/s, and take an *in situ* image 3.5 ms after the end of the ramp. At the boundaries of the bistable region, the density of the system becomes discontinuous. Experimentally, we observe that the self-bound state cannot adjust to this abrupt change and fragments, see right panel. To locate the fragmentation point, we record the atom number in the initially self-bound region and observe an abrupt drop at a critical magnetic field. As shown in the left panel of Fig. 4(a), its value depends on the initial atom number. We summarize the position of the fragmentation point in the N-B plane in Fig. 4(b).

We exploit the variational model to interpret our observations. According to it, although in the bistable region both solitons and droplets exist, their energies coincide only along a transition line (solid line). Above (below) it, solitons (droplets) become metastable, and only disappear at the upper (lower) boundary (dashed lines). The three situations are depicted in the right panel of Fig. 4(b). Experimentally, we prepare the mixture in a regime where only solitons exist. Therefore, when entering the bistable region we expect it to follow preferentially the metastable soliton solution, with which it connects smoothly. At the upper boundary the metastable soliton disappears and only dense droplets are possible. Hence, the system is expected to fragment and form an excited state with identical total energy. A similar behavior is observed in trapped dipolar gases [11,22,47,48]. Our experimental results support this hypothesis: within error bars, the fragmentation point agrees with the upper boundary of the bistable region predicted by the variational (solid line) and numerical EGPE (colored area) calculations without any fitting parameters.

In conclusion we have shown that an attractive mixture of BECs confined in an optical waveguide always hosts self-bound states, which correspond to composite bright solitons, quantum liquid droplets, or interpolate smoothly between both limits depending on the values of the atom number, interaction strength, and confinement. We have

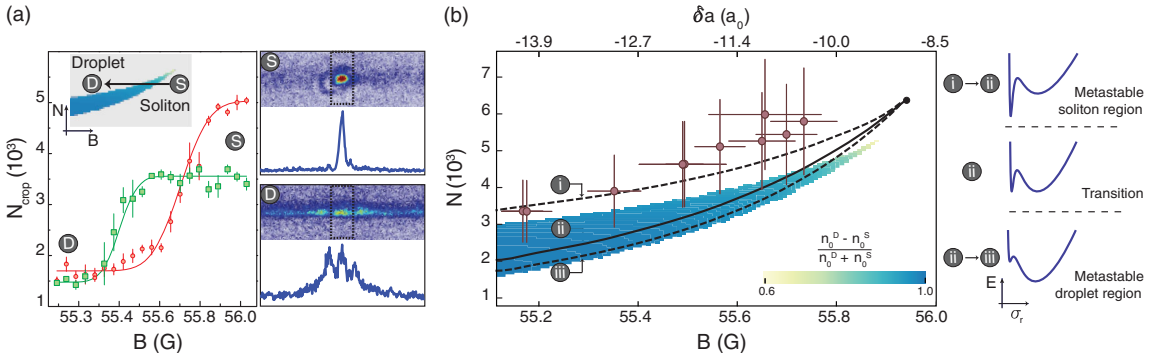

FIG. 4. Soliton-to-droplet transition. (a) Left panel: Atom number in the self-bound region N_{crop} as a function of magnetic field B when approaching the bistable region from the soliton regime, see inset. Top right panel: Initial soliton image (S) and corresponding doubly integrated density profile. Bottom right panel: Fragmentation observed when entering the droplet regime (D). (b) Measured fragmentation point vs N and B. Error bars: Systematic error in N and magnetic field width of the fragmentation curve [25]. Colored area: Bistable region computed numerically from the EGPE. Lines: Variational model, indicating the boundaries of the bistable region (dashed) and the transition line where solitons and droplets have identical energies E (solid). Insets: Sketch of E vs σ_z for the metastable soliton and droplet regions and the transition line.

characterized their spin composition and density, and mapped out the upper boundary of the bistable region separating solitons and droplets. Future experimental directions include the study of metastability and hysteresis when crossing the soliton-to-droplet transition from different directions. Another interesting possibility is to perform collisions between two self-bound states, which are expected to display very different behavior in the soliton and droplet limits [13,49,50]. Finally, spin imbalanced systems offer the possibility to explore finite temperature effects [51] in a well controlled setting, exploiting the excess component as a thermal bath.

We thank P. Naylor for technical assistance with the numerical simulations, and A. Celi and P. Thomas for a careful reading of the Letter. We acknowledge insightful discussions with G. Astrakharchik, J. Boronat, M. Fattori, I. Ferrier-Barbut, B. Malomed, D. Petrov, L. Santos, G. Semeghini, and L. Torner. We thank A. Simoni and M. Tomza for calculations of the potassium scattering lengths. We acknowledge funding from Fundació Privada Cellex, EU (MagQUPT-631633 and QUIC-641122), Spanish MINECO (StrongQSIM FIS2014-59546-P and Severo Ochoa SEV-2015-0522), DFG (FOR2414), Generalitat de Catalunya (SGR874 and CERCA program), and Fundación BBVA. P. C. acknowledges support from the Marie Skłodowska-Curie actions (TOPDOL-657439), C. R. C. from CONACYT (402242/384738), J. S. from FPI (BES-2015-072186), and L. Tarruell from the Ramón y Cajal program (RYC-2015-17890).

Note added.—Recently, we became aware of related experiments by the LENS group [52].

*leticia.tarruell@icfo.eu

[1] T. Dauxois and M. Peyrard, *Physics of Solitons* (Cambridge University Press, Cambridge, England, 2006).
[2] B. A. Malomed, D. Mihalache, F. Wise, and L. Torner, J. Opt. B **7**, R53 (2005).
[3] M. Barranco, R. Guardiola, S. Hernández, R. Mayol, J. Navarro, and M. Pi, J. Low Temp. Phys. **142**, 1 (2006).
[4] K. E. Strecker, G. B. Partridge, A. G. Truscott, and R. G. Hulet, Nature (London) **417**, 150 (2002).
[5] L. Khaykovich, F. Schreck, G. Ferrari, T. Bourdel, J. Cubizolles, L. D. Carr, Y. Castin, and C. Salomon, Science **296**, 1290 (2002).
[6] P. Medley, M. A. Minar, N. C. Cizek, D. Berryrieser, and M. A. Kasevich, Phys. Rev. Lett. **112**, 060401 (2014).
[7] S. L. Cornish, S. T. Thompson, and C. E. Wieman, Phys. Rev. Lett. **96**, 170401 (2006).
[8] A. L. Marchant, T. P. Billam, T. P. Wiles, M. M. H. Yu, S. A. Gardiner, and S. L. Cornish, Nat. Commun. **4**, 1865 (2013).
[9] G. D. McDonald, C. C. N. Kuhn, K. S. Hardman, S. Bennetts, P. J. Everitt, P. A. Altin, J. E. Debs, J. D. Close, and N. P. Robins, Phys. Rev. Lett. **113**, 013002 (2014).
[10] S. Lepoutre, L. Fouché, A. Boissé, G. Berthet, G. Salomon, A. Aspect, and T. Bourdel, Phys. Rev. A **94**, 053626 (2016).
[11] H. Kadau, M. Schmitt, M. Wenzel, C. Wink, T. Maier, I. Ferrier-Barbut, and T. Pfau, Nature (London) **530**, 194 (2016).
[12] I. Ferrier-Barbut, H. Kadau, M. Schmitt, M. Wenzel, and T. Pfau, Phys. Rev. Lett. **116**, 215301 (2016).
[13] I. Ferrier-Barbut, M. Schmitt, M. Wenzel, H. Kadau, and T. Pfau, J. Phys. B **49**, 214004 (2016).
[14] M. Schmitt, M. Wenzel, F. Böttcher, I. Ferrier-Barbut, and T. Pfau, Nature (London) **539**, 259 (2016).
[15] L. Chomaz, S. Baier, D. Petter, M. J. Mark, F. Wächtler, L. Santos, and F. Ferlaino, Phys. Rev. X **6**, 041039 (2016).
[16] C. R. Cabrera, L. Tanzi, J. Sanz, B. Naylor, P. Thomas, P. Cheiney, and L. Tarruell, Science **359**, 301 (2018).
[17] D. S. Petrov, Phys. Rev. Lett. **115**, 155302 (2015).
[18] V. M. Pérez-García, H. Michinel, and H. Herrero, Phys. Rev. A **57**, 3837 (1998).
[19] L. Salasnich, A. Parola, and L. Reatto, Phys. Rev. A **66**, 043603 (2002).
[20] L. D. Carr and Y. Castin, Phys. Rev. A **66**, 063602 (2002).
[21] F. Wächtler and L. Santos, Phys. Rev. A **94**, 043618 (2016).
[22] R. N. Bisset, R. M. Wilson, D. Baillie, and P. B. Blakie, Phys. Rev. A **94**, 033619 (2016).
[23] C. C. Bradley, C. A. Sackett, and R. G. Hulet, Phys. Rev. Lett. **78**, 985 (1997).
[24] S. Roy, M. Landini, A. Trenkwalder, G. Semeghini, G. Spagnolli, A. Simoni, M. Fattori, M. Inguscio, and G. Modugno, Phys. Rev. Lett. **111**, 053202 (2013).
[25] See Supplemental Material at http://link.aps.org/supplemental/10.1103/PhysRevLett.120.135301 for additional information on scattering lengths, inelastic losses, theoretical analysis, and data analysis, which includes as well Refs. [26–36].
[26] C. D'Errico, M. Zaccanti, M. Fattori, G. Roati, M. Inguscio, G. Modugno, and A. Simoni, New J. Phys. **9**, 223 (2007).
[27] A. Simoni (private communication).
[28] S. Falke, H. Knöckel, J. Friebe, M. Riedmann, E. Tiemann, and C. Lisdat, Phys. Rev. A **78**, 012503 (2008).
[29] M. Tomza (private communication).
[30] T. Weber, J. Herbig, M. Mark, H.-C. Nägerl, and R. Grimm, Phys. Rev. Lett. **91**, 123201 (2003).
[31] M. Zaccanti, B. Deissler, C. D'Errico, M. Fattori, M. Jona-Lasinio, S. Mller, G. Roati, M. Inguscio, and G. Modugno, Nat. Phys. **5**, 586 (2009).
[32] D. M. Larsen, Ann. Phys. (N.Y.) **24**, 89 (1963).
[33] X. Antoine and R. Duboscq, Comput. Phys. Commun. **185**, 2969 (2014).
[34] C. J. Pethick and H. Smith, *Bose-Einstein Condensation in Dilute Gases* (Cambridge University Press, Cambridge, England, 2008).
[35] D. Petrov and L. Santos (private communication).
[36] Yu. Kagan, B. V. Svistunov, and G. V. Shlyapnikov, JETP Letters **42**, 209 (1985).
[37] The system decoheres rapidly after the rf pulse, forming a two-component mixture.
[38] D. S. Hall, M. R. Matthews, J. R. Ensher, C. E. Wieman, and E. A. Cornell, Phys. Rev. Lett. **81**, 1539 (1998).
[39] Although the beam also creates a longitudinal confinement of frequency $\omega_z/2\pi \lesssim 1$ Hz along its propagation direction,

it is insufficient to trap the atoms due to a residual tilt with respect to the horizontal axis.
[40] D. S. Petrov and G. E. Astrakharchik, Phys. Rev. Lett. **117**, 100401 (2016).
[41] The system minimizes its energy by maximizing the overlap of the two components, justifying the assumption of identical spatial modes.
[42] T. D. Lee, K. Huang, and C. N. Yang, Phys. Rev. **106**, 1135 (1957).
[43] For our experimental parameters, a_{ho} exceeds the healing length of each BEC by more than an order of magnitude.
[44] V. M. Pérez-García, H. Michinel, J. I. Cirac, M. Lewenstein, and P. Zoller, Phys. Rev. A **56**, 1424 (1997).
[45] A related behavior, involving a bistable region and a crossover regime, has been studied in harmonically trapped dipolar gases [21,22]. In this case, the low- and high-density solutions correspond to a BEC and a quantum droplet.
[46] For all the measurements, the droplet and soliton sizes remain below (or are comparable to) the spatial resolution of the imaging system.
[47] I. Ferrier-Barbut, M. Wenzel, M. Schmitt, F. Böttcher, and T. Pfau, Phys. Rev. A **97**, 011604(R) (2018).
[48] F. Wächtler and L. Santos, Phys. Rev. A **93**, 061603(R) (2016).
[49] J. H. V. Nguyen, P. Dyke, D. Luo, B. A. Malomed, and R. G. Hulet, Nat. Phys. **10**, 918 (2014).
[50] S. K. Adhikari, Phys. Rev. A **95**, 023606 (2017).
[51] A. Boudjemaa, Ann. Phys. (Amsterdam) **381**, 68 (2017).
[52] G. Semeghini, G. Ferioli, L. Masi, C. Mazzinghi, L. Wolswijk, F. Minardi, M. Modugno, G. Modugno, M. Inguscio, and M. Fattori, arXiv:1710.10890.